IEEE Access
Multidisciplinary | Rapid Review | Open Access Journal

Received December 12, 2020, accepted December 23, 2020, date of publication December 30, 2020,
date of current version January 8, 2021.

Digital Object Identifier 10.1109/ACCESS.2020.3048117

Design of a Novel Fully Automatic Ocean Spectra Acquisition and Control System Based on the Real-Time Solar Angle Analyzing and Tracking

LEI YANG[1,2], HAO GAO[2,3], DINGFENG YU[1,2,4], (Member, IEEE), SHUNQI PAN[5], YAN ZHOU[1,2], AND YINGYING GAI[1,2]

[1]Institute of Oceanographic Instrumentation, Qilu University of Technology (Shandong Academy of Sciences), Qingdao 266100, China
[2]National Engineering and Technological Research Center of Marine Monitoring Equipment, Qingdao 266100, China
[3]College of Geodesy and Geomatics, Shandong University of Science and Technology, Qingdao 266590, China
[4]Key Laboratory of Tropical Oceanography, South China Sea Institute of Oceanology, Chinese Academy of Sciences, Guangzhou 510301, China
[5]Hydro-Environmental Research Centre, School of Engineering, Cardiff University, Cardiff CF24 3AA, U.K.

Corresponding authors: Dingfeng Yu (dfyu@qlu.edu.cn) and Hao Gao (haog@fio.org.cn)

This work was supported in part by the National Key Research and Development Program of China under Project 2017YFC1404802, in part by the Key Research and Development Program of Shandong under Project 2019GHY112017, in part by the State Key Laboratory of Tropical Oceanography, South China Institute of Oceanology, Chinese Academy of Sciences, under Project LTO2017, in part by the Shandong Province Youth Innovation and Technology Program under Project 2019KJN009, in part by the Open Research Fund of the State Key Laboratory of Estuarine and Coastal Research under Project SKLEC-KF202001, and in part by the National Natural Science Foundation of China under Project 61701287.

ABSTRACT The current manual spectra acquisition for monitoring water constituents has resulted in discontinuous data acquisition, insufficient amount of data, and small ocean coverage. This article presents the design of a novel fully automatic ocean spectra acquisition and control system based on the real-time solar angle analyzing and tracking. To ensure that the requirements for spectra acquisition are met, the system is capable of accurately calculating the solar angle by collecting the information of latitude, longitude, date, time and direction, and automatically adjusting the position of instrument observation plane and the pointing angle of fiber optic probe in real-time. It achieves full automation of collecting the downward radiance of skylight, the upward radiance from reference panel and seawater separately through controlling the rotation of fiber optic probe. A 188-day observation experiment was carried out at the coastal ocean experimental station in Qingdao from September 11, 2018 to March 17, 2019. After that, the system was conducted onboard the Dongfanghong 3 scientific research vessel for a one-month demonstration and sea trial in June 2019. Comparative experiments including manual spectra collection, chlorophyll-a sensor measurement, and water samples collection were carried out. The experimental results show that the relative error of the spectra between the system and manual collection is less than 5%, and the relative error of the remote sensing reflectance calculated by the spectra is less than 4%. Considering the chlorophyll-a concentration obtained by the sensor and the water samples as the true value, the relative error of the chlorophyll-a concentration obtained by the system is 10% and 25% respectively. The results show its full and reliable capacity in collecting spectra of seawater automatically and continuously in real-time, with satisfactory accuracy and timeliness.

INDEX TERMS Spectra acquisition, automatic control system, solar angles, chlorophyll-a, ocean color.

I. INTRODUCTION

With the rapid economic and technological development in China, the improvement of marine undertakings becomes more important and many breakthroughs have been made in ocean research in recent years. Determining and understanding water constituents play a fundamental role in marine science, especially for monitoring changes in ocean waters and risk analysis of marine ecosystems [1]–[3]. For example, estimating concentrations of chlorophyll-a (Chl-a), suspended particulate matter (SPM), and colored dissolved organic matter (CDOM) through traditional

The associate editor coordinating the review of this manuscript and approving it for publication was Nishant Unnikrishnan.

spectral collection method commonly relies on manual spectral collection and measurement [4]. However, manually controlled spectral collection can be very difficult for continual and long-term measurements [5]. Furthermore, due to the complex and harsh marine environment where the measurements are taken, manual spectra acquisition can often be disrupted and inefficient, which can be a significant hurdle in the development and application of marine hyperspectral remote sensing technology [6]–[8]. Therefore, it is urgently required to develop an automatic and reliable ocean spectra acquisition system to provide high quality data for accurate and long-term assessment of the marine ecosystem.

In order to achieve the full automation of spectra acquisition, it is necessary to develop a system that is capable of automatically identifying and tracking the solar angle for real-time adjustment of the pointing position of instrument probe with an efficient and stable workflow [9]. In recent years, there have been a number of studies on solar tracking, which is primarily used in system navigation and positioning [10], weather forecast [11], improvement of the efficiency of photovoltaic power generation [12], and solar radiation thermal energy accumulation [13]. In terms of the automatic tracking and collection of the solar spectrum, Li *et al.* studied the automatic tracking device of the solar spectral irradiance instrument [14]. Chen *et al.* developed the automatic spectra acquisition system based on solar tracking [15]. However, these studies only focus on the automatic collection of the solar spectrum, and have not been applied to the spectra collection of ocean color inversion. The Canadian Satlantic Company designed the HyperSAS sea surface height spectrometer to collect the ocean spectra [16]. The spectrometer has realized the collection of ocean spectra but has not realized the full automation of collection [17]. The Shanghai Yiwin Instrument Equipment Co., LTD proposed and designed the Above-Water Radiance Auto Measuring System [18], it realizes the automatic collection of ocean spectra [19], but it can not automatically adjusting the position of instrument observation plane and the pointing angle of probe according to the solar angle in real-time.

To this end, a novel fully automatic ocean spectra acquisition and control system based on the real-time solar angle analyzing and tracking is proposed in this article, aiming to address the difficulties experienced in continuous data acquisition, as well as the quantity and coverage of the data required with the manual spectra acquisition. Compared with the existing system, the contributions of the novel system is shown in TABLE 1.

The important contributions of this article are summarized as follows:

1. The overall design and structure of the system, which include the data acquisition and control subsystem; and the mechanical supporting rotation subsystem, with the description of the fully automatic workflow of the system.

2. The algorithm for analyzing and tracking of the solar angle in real-time, which ensures that the system meets the geometric requirements for water spectra observation and acquisition in any case. It also ensures the optimal realization of the system's adjustment of the instrument position and fiber optic probe.

3. The 188-day coastal experiments at a nearshore station and the 30-day vessel-mounted onboard experiments, which are conducted to evaluate the performance of this system. During the experiments, comparative experiments including manual spectra collection, direct Chl-a sensor measurements and water samples collection were carried out to evaluate the reliability, validity and accuracy of the system.

TABLE 1. Contributions compared to other systems.

	HyperSAS sea surface height spectrometer	Above-Water Radiance Auto Measuring System	Novel Fully Automatic Ocean Spectra Acquisition and Control System
Collection of ocean spectra	Yes	Yes	Yes
Automation of collection	No	Yes	Yes
Adjusting the position of instrument observation	No	No	Yes
Adjusting the pointing angle of probe	No	No	Yes

The remainder of this article is organized as follows. The overall design of the structure of the system is presented in Section 2. The calculation process of the solar angle is introduced in Section 3. The simulation and analysis of solar azimuth variation are detailed in Section 4. The results of the experiments in coastal and open sea waters are given in Section 5, followed by the conclusions in Section 6.

II. OVERALL DESIGN OF THE SYSTEM

A. SYSTEM STRUCTURE

The fully automatic ocean spectra acquisition and control system consists of data acquisition and control subsystem and mechanical supporting rotation subsystem. The data acquisition and control subsystem is designed to receive and process the sensor data, to generate the hardware driving instructions such as rotating motor and steering gear. It mainly consists of spectrometer, industrial control computer (upper computer system), circuit control board (Micro Control Unit (MCU) lower computer system), and power supply. The mechanical supporting rotation subsystem is to provide support and rotation control of the observation part, and consists of reference panel, fiber optic steering gear, sun follower turntable, fiber optic probe, camera, and related support columns. The overall schematic structure diagram of the system is shown in Fig.1.

1) DATA ACQUISITION AND CONTROL SUBSYSTEM

The schematic structure diagram of the data acquisition and control subsystem is shown in Fig.2. It is mainly designed

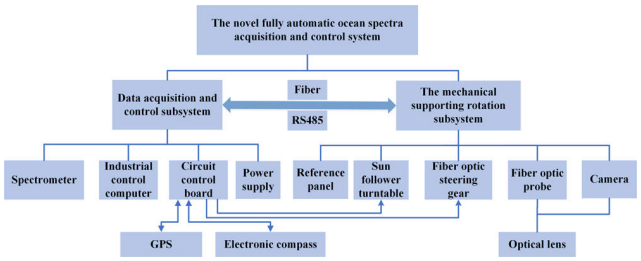

FIGURE 1. The schematic diagram of the overall design and structrure of the system.

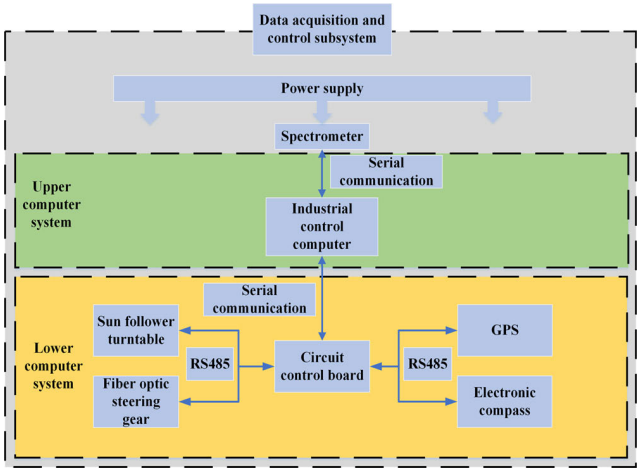

FIGURE 2. The schematic structure diagram of the data acquisition and control subsystem.

to achieve four functions, namely sensors data receiving and processing, calculation of the solar angle, analysis of instrument observation position and probe pointing, and driving the rotating motor and optical fiber steering gear to rotate. In particular, the Global Positioning System (GPS) module provides the latitude and longitude of the spectral acquisition location. It also provides the date and time of the spectral acquisition. The compass provides the direction information that indicates the initial azimuth of the instrument in which the optical fiber probe is located. The camera takes pictures to record the environment when the spectra is collected, which can ensure the data affected by shadows is deleted during data processing. The data acquisition and control subsystem calculates the angle of the sun in real-time according to the processing result of latitude, longitude, date, and time information. Based on the real-time calculation of the solar angle, the observation plane position of instrument and the pointing angle of the optical fiber steering gear are then determined.

2) MECHANICAL SUPPORTING ROTATION SUBSYSTEM

The mechanical supporting rotation subsystem provides the support and rotation function of the reference panel, fiber optic probe, camera, fiber optic steering gear, and the sun-tracking turntable. It ensures the whole system to execute the rotation and collection instruction issued by the data acquisition and control subsystem stably and reliably. The schematic diagram of the mechanical supporting rotation subsystem is shown in Fig.3. The turntable motor is used to achieve the real-time rotation of the instrument observation plane. The optical fiber steering gear could execute the directional control when the optical fiber probe collects the spectra of the skylight, seawater and reference panel. The fiber optic probe and camera are fixed in the protection objective, which could provide necessary protection and prevent condensation of water vapor on probe and salt spray corrosion from affecting data acquisition processing. Support columns, fixtures, and connectors ensure the reliability and stability of the whole instrument system.

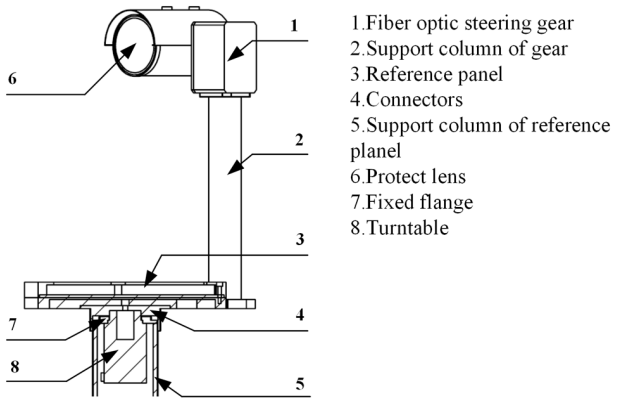

FIGURE 3. The schematic diagram of the mechanical supporting rotation subsystem.

B. SYSTEM FUNCTION REALIZATION

The prototype of the system is shown in Fig.4. The data acquisition and control subsystem is designed to calculate the angle of the sun in real-time, according to the latitude, longitude, date, and time information received. Then the analysis of the position of the instrument observation plane and the pointing angle of the optical fiber steering gear are carried out, according to the geometric requirements for water spectra

FIGURE 4. The prototype of the designed system.

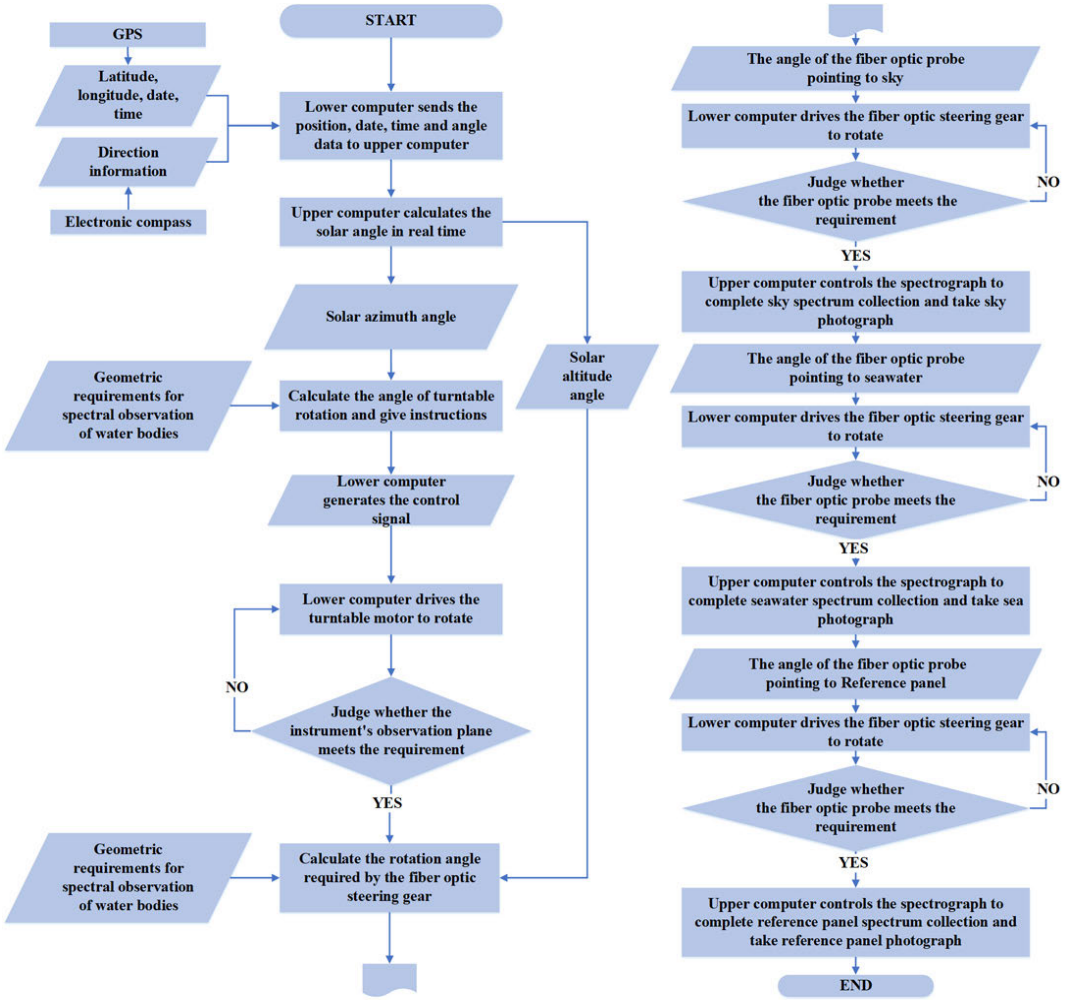

FIGURE 5. The prototype of the designed system.

observation. The result of the desired position and angle are then sent to the turntable motor and fiber optic steering gear respectively via a RS485 communication protocol.

After receiving the position and angle information sent from the data acquisition and control subsystem, the turntable motor in the mechanical supporting rotation subsystem controls the rotation of the instrument in real-time, which ensures that the instrument observation plane for spectral collection always meets the angle required by the geometry of water spectral observation. Then the fiber optic steering gear controls the fiber optic probe to rotate to point to the sky, seawater and reference panel respectively for collecting the required spectral information, based on the geometric requirements of water spectra observation. The workflow diagram of the system is given in Fig.5.

III. SOLAR ANGLE CALCULATION

The angle of the sun is calculated in real-time based on the latitude, longitude, date and time information received [20]. The solar angle is calculated by the MCU lower computer control system and upper computer system. The calculation process is shown in Fig.6.

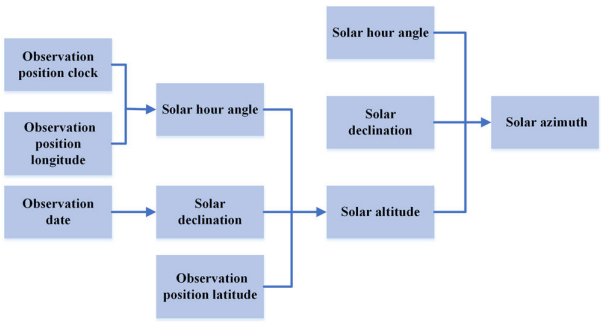

FIGURE 6. The flow chart of solar angle calculation.

A. SOLAR HOUR ANGLE CALCULATION

As China sits in UTC+08:00 time zone (i.e. eight hours ahead of Coordinated Universal Time), a single standard time offset is used. The time stamp is set as the true solar time, rather than using Beijing Time in the analysis. Therefore, when calculating the azimuth of the sun, it is necessary to calculate the true solar time of the geographical position at first [21] as expressed as [22], [23]:

$$T_{sun} = T_{clock} + (L_e - 120)/15 \quad (1)$$

where is the true solar time at the observation location and L_e is the longitude of the location. After the true solar time is set, the current solar hour angle of the location (A_{sun}) can be calculated as [23], [24]:

$$A_{sun} = (T_{sun} - 12) \times 15 \tag{2}$$

B. SOLAR DECLINATION CALCULATION

The declination of the sun is the latitude of the direct point of the sun, which varies with date. There are several methods to calculate the declination of the sun depending on the accuracy required. Here, the Bourges algorithm proposed in [22], which has the highest accuracy in all solar declination formulae, is used as [22], [25]:

$$\begin{aligned}\delta = {} & 0.3723 + 23.2567\sin(\omega t) \\ & + 0.1149\sin(2\omega t) - 0.1712\sin(3\omega t) - 0.7580\cos(\omega t) \\ & + 0.3656\cos(2\omega t) + 0.0201\cos(3\omega t)\end{aligned} \tag{3}$$

where

$$\omega = 2\pi \big/ 365.2422 \tag{4}$$

$$t = dn - 1 - n_0 \tag{5}$$

$$\begin{aligned}n_0 = {} & 78.801 + [0.2422(year - 1969)] \\ & - round[0.25(year - 1969)]\end{aligned} \tag{6}$$

where in Eq. (5), dn represents the nth day of the year (from 1 to 365 in common years, and 1 to 366 in leap years).

C. SOLAR ALTITUDE ANGLE CALCULATION

The solar altitude angle refers to the angle between the rays of the sun at a given location and the section of the earth's surface connected to the center of the earth by that location. Time is the main factor to determine the solar altitude angle at the location. The solar altitude angle reaches its minimum of zero at both sunrise and sunset, and reaches its maximum of 90° at noon during the day. Therefore, the calculation of the solar altitude angle requires the geographic latitude information of the observing ground, solar declination information calculated by date, and the information of the solar hour angle calculated according to the time of the day, with the following expression [23], [26]:

$$h_{sun} = \arcsin\{\sin(L_l)\times\sin(\delta) - \cos(L_l)\times\cos(\delta)\times\cos(A_{sun})\} \tag{7}$$

where L_l is the geographic latitude information of the observed location.

D. SOLAR AZIMUTH CALCULATION

Solar azimuth refers to the angle between the projection of the sun's rays on the ground and the local meridian. It is also defined as the angle measured in the clockwise direction, which should start with the north direction of the target object and end with the incident direction of the sunlight [25], [27], [28]. In this article, for the convenience of calculation, the south direction of the object is chosen as the starting direction. When the solar azimuth is south by east in the morning, the value would be negative. When the solar azimuth is south-west in the afternoon, its value is positive. The solar azimuth calculation is given below:

$$\theta_{sun} = \arcsin\{\cos(\delta) \times \sin(A_{sun}) / \cos(h_{sun})\} \tag{8}$$

E. ANALYSIS OF INSTRUMENT OBSERVATION PLANE AND FIBER OPTIC PROBE POINTING

The analysis processing of geometric requirements for water spectra observation is shown in Fig.7. As an example, plane ABCD is the observation plane of the instrument, and plane EFGH is the incident plane of sunlight. AO refers to the pointing of the fiber optic probe when measuring the upward radiance from the reference panel. AW refers to the pointing of the fiber optic probe when measuring the upward radiance from seawater. AK, which is located in the ABCD plane, refers to the pointing of the fiber optic probe when measuring the downward radiance of skylight. During the observation and measurement, it is generally required that the angle between the observation plane of the instrument and the incident plane of the sunlight is about 135° [29], [30], namely ∠COH=135°. In addition, the values of both ∠CAO and ∠CAW are between 30°and 60°, respectively [31]. By setting the observation angle in this way, the influence of direct sunlight and reflection could be minimized [32], [33], and the collected spectra could be avoided from being saturated [34], [35].

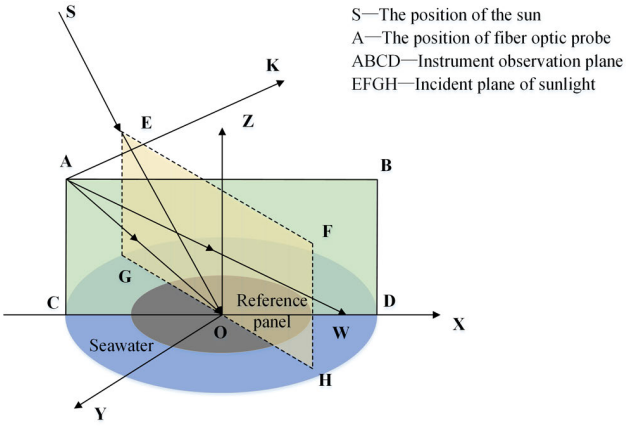

FIGURE 7. Schematic diagram of geometric requirements for water spectra observation.

IV. THE SIMULATION AND ANALYSIS OF SOLAR AZIMUTH VARIATION

This proposed system is intended to achieve the full automation of collecting ocean spectral information to derive the concentration of Chl-a, SPM, and CDOM for marine environmental monitoring and hydrologic analysis. Generally, in Case I waters [1], concentrations of Chl-a are relatively small and stable in a short time, and SPM and CDOM are very low and essentially non-measurable. In Case II waters, the concentrations of Chl-a, SPM, and CDOM are much

higher and the optical properties are complex, which are most suitable for the system to apply. Therefore, in this study, applications of the system to the Case II waters of China are demonstrated.

A. ANALYSIS OF SOLAR AZIMUTH VARIATION IN DIFFERENT CHINESE SEAS

To validate the algorithm for determining the solar azimuth as described in the previous sections, four observation locations located in the Bohai Sea, the Yellow Sea, the East China Sea, and the South China Sea are selected in this study. The latitudes and longitudes of the observation locations are given in Table 2 and illustrated in Fig.8.

TABLE 2. Latitudes and longitude of four observation locations.

Location	Longitude	Latitude
1 Bohai Sea	120.009195°	38.741108°
2 Yellow Sea	121.640625°	35.101934°
3 East China Sea	122.563476°	27.586197°
4 South China Sea	109.885877°	17.908004°

FIGURE 8. Observation locations in the Bohai Sea (1), the Yellow Sea (2), the East China Sea (3), and the South China Sea (4), respectively.

Fig.9 shows the calculated solar azimuth by the system on September 1, 2019 from 9:00 to 16:00 from those locations. The results show that at the same observation time during the day, the variation of solar azimuth in the different locations with time are different. For the Bohai Sea and the Yellow Sea, which are geographically close and have the higher latitudes, the trend of solar azimuth variation is close and also tends to relatively linear. In the South China Sea, which is at the lowest geographic latitude, the variation of solar azimuth is the largest compared with those at the other three locations, exhibiting a strong non-linearity, while the solar azimuth variation in the East China Sea is in between. From Fig.9, it is evident that the sequence of the time when the solar azimuth reaches zero at the four observation positions is the same as the order of their longitudes from large to small, which are

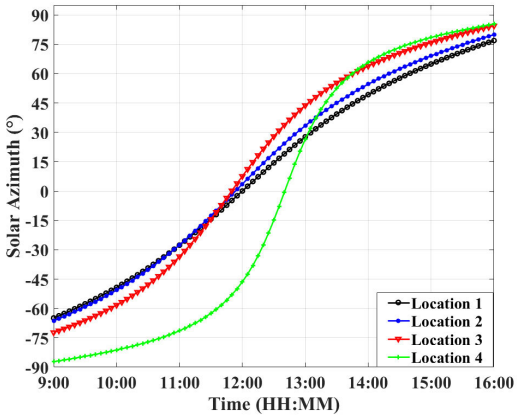

FIGURE 9. Variations of solar azimuth with time in different offshore areas of China.

the East China Sea, the Yellow Sea, the Bohai Sea, and the South China Sea.

To further analyze the influence of longitude and latitude on the variation of solar azimuth, seven locations along transects of longitude of 120°E and latitude of 60°N as detailed in Table 3 are selected and used. As shown in Fig.10, the transect of (A-B-C-D) is designed to examine the influence of latitude on the solar azimuth, and other transect (E-F-B-G) is to examine the longitudinal influence.

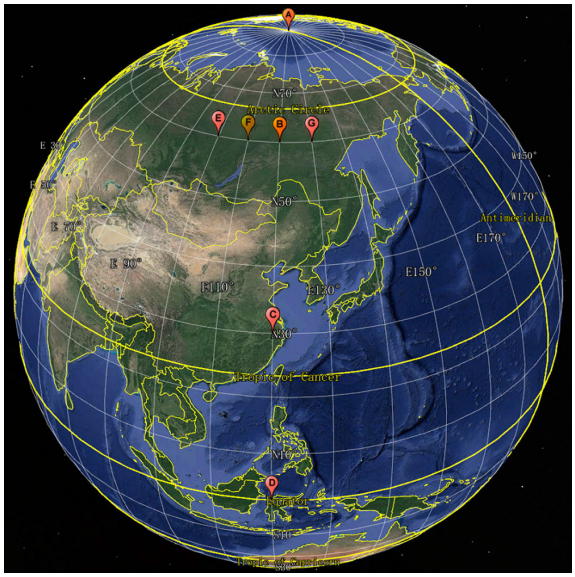

FIGURE 10. Seven observation locations (A-B-C-D-E-F-G). A-B-C-D indicate four observation locations at the same longitude (120°E), but different latitudes. E-F-B-G indicate four observation locations at the same latitude (60°N), but different longitudes.

Fig.11 shows the simulation from 9:00 to 15:00 on September 1, 2019. As can be seen from the simulation results, under the same longitude (Fig.11 (a)), the change of latitude affects the variation of the solar azimuth. The higher the latitude is, the more linear the trend of the solar azimuth during the day shows. At low latitudes, the azimuth of the

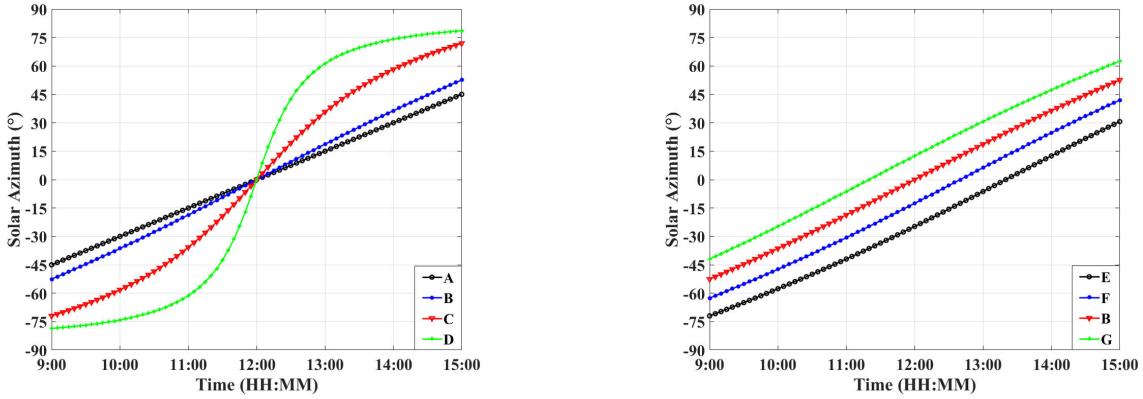

(a) Longitude of 120°E (A-B-C-D)

(b) Latitude of 60°N (E-F-B-G)

FIGURE 11. Variations of solar azimuth along latitudes and latitude (60°N).

TABLE 3. Details of observation locations.

Location	Longitude	Latitude
A	120°	90°
B	120°	60°
C	120°	30°
D	120°	0°
E	100°	60°
F	110°	60°
G	130°	60°

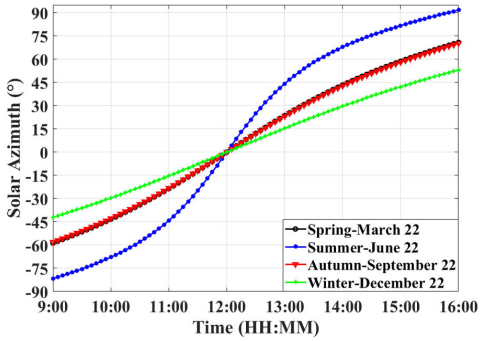

FIGURE 12. Variations of solar azimuth through a day at Location 1 (in the Bohai Sea) in different seasons.

sun changes faster as it approaches noon, and slower as it approaches morning and evening. However, under the same latitude (Fig.11 (b)), with the change of longitude, the variation of the solar azimuth is unchanged. There is only the case of arriving at the same solar azimuth earlier or later between different longitudes. The lower the longitude, the longer the delay time.

B. ANALYSIS OF SOLAR AZIMUTH VARIATION IN DIFFERENT SEASONS

The solar azimuth in different seasons of the year is simulated and analyzed at the observation locations in the Bohai Sea on March 22, June 22, September 22, and December 22, 2019 to represent spring, summer, autumn and winter seasons. As shown in Fig.12, the variation of the solar azimuth in spring and autumn seasons is basically identical. The variation of solar azimuth in winter is the most linear, while the variation of solar azimuth in summer is the least linear. The seasonal influence on the tendency of the solar azimuth exhibits a similar pattern as that of latitude. The latitude of the direct point of the sun is different in different seasons. For the same fixed observation location, the latitude difference between the observation location and the point of direct sunlight is different among seasons. Since the observation location is in the Bohai Sea (northern hemisphere), the distance between the observation location and the direct point is the largest in winter and the latitude difference is the largest. While the distance between the observation location and the direct point is the smallest in summer and the latitude difference is the smallest. This result is also consistent with the analysis of the same longitude in section 4.1, the higher the latitude, the more linear the trend of the solar azimuth is, while the lower the latitude, the less linear the trend of the solar azimuth is.

Considering the variation patterns of solar azimuth obtained from the simulations, the azimuth adjustment of the system can be set with specific strategies. In particular, when the observation position is located in the high latitude sea area or the observation is undertaken in summer season, the azimuth of the sun changes slowly in the morning and evening, and the azimuth changes rapidly at noon. In this case, the system can be controlled to adjust the observation angles at long intervals in the morning and evening, and once at short intervals at noon. This system control strategy not only ensures the accuracy and precision of angle adjustment, but also saves the power consumption of excessive times of system adjustment in the morning and evening. When the observation location is in the low latitude sea area or when the

(a) Coastal ocean experimental station in Qingdao

(b) Dongfanghong 3 scientific research vessel

FIGURE 13. The experimental locations of the system.

observation season is in the winter season, the change of solar azimuth tends to be linear, and the change of solar azimuth angle in the same time is almost equal. The adjustment of the angle of the system can be set with a fixed value, to avoid the complex calculation process of the system and improve the adjustment efficiency of the system.

V. EXPERIMENTAL VERIFICATION OF THE SYSTEM

The system was tested by a plethora of experiments in coastal and open sea waters. Firstly, the system was tested with the laboratory facilities over a 188-day period for spectra acquisition at the coastal ocean experimental station in Qingdao from September 11, 2018 to March 17, 2019 (Fig.13 (a)). The coastal ocean experimental station is part of the research facilities of the Institute of Oceanographic Instrumentation, Shandong Academy of Sciences, which is well regarded as the only comprehensive coastal ocean experimental station in China and provides long-term and reliable offshore experimental conditions for various types of scientific instruments.

Secondly, the system was taken onboard the Dongfanghong 3 research vessel for carrying out in situ spectra collection and water sample collection experiments between May 31, 2019 and June 30, 2019 (Fig.13 (b)). The Dongfanghong 3 is a comprehensive marine scientific research vessel with a displacement of 5000 tons, which is the first in China and the fourth in the world to have the Silent-R certified. It is also the largest in the world to obtain the Silent-R certificate. It was very fortunate that the sea trial for spectra acquisition and water sample collection experiments in this study were conducted.

The experimental sampling locations of the coastal station and Dongfanghong 3 are shown in the Fig.14.

It is considered that the water bodies in the sea trial area are representative, because the coastal waters near Shanghai and Xiamen are regarded as Case II waters, with poor water quality and high contents of Chl-a, SPM and CDOM, while the waters in the South China Sea are Case I waters. The water quality is clear, the Chl-a content is low, and there is almost no SPM or CDOM. The water quality of the East China Sea is somewhere in between. The voyage route covered the entry from Case II waters into Case I waters and the entry from Case I waters into Case II waters. The conditions helped intuitively assess whether the system measures accurately.

A large number of data sets of spectra, water samples, and Chl-a sensor were obtained during the system verification tests, details of which are listed in Table 4.

TABLE 4. Details of observation locations.

Category	Sources	Amount	Fetch time
Spectral data	Coastal ocean experimental station	26320	From September 11, 2018 to March 17, 2019
	Dongfanghong 3 scientific research vessel	4340	From May 31, 2019 to June 30, 2019
Water samples	Coastal ocean experimental station	30	From March 13, 2019 to March 17, 2019
	Dongfanghong 3 scientific research vessel	52	From June 9, 2019 to June 28, 2019
Sensor data	Coastal ocean experimental station	27936	From November 19, 2018 to November 26, 2018 From January 22, 2019 to January 29, 2019
	Dongfanghong 3 scientific research vessel	19490	From June 15, 2019 to June 18, 2019 From June 22, 2019 to June 28, 2019

Remote sensing reflectance (Rrs) is defined as the ratio of water-leaving radiance to downwelling irradiance just above

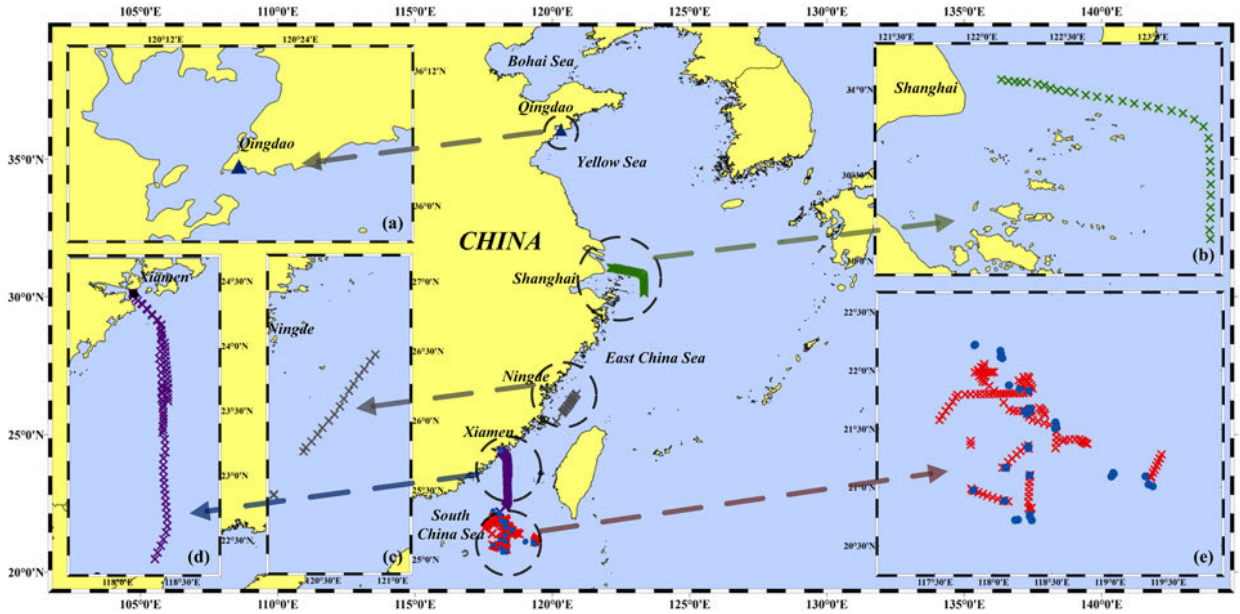

FIGURE 14. Schematic diagram of sampling locations of the sea trials: (a) sampling location in the coastal waters of Qingdao; (b-e) routes of the sea trials onboard Dongfanghong 3: from Shanghai to Xiamen in the offshore waters of Shanghai; from Shanghai to Xiamen in the offshore waters of Ningde; from Xiamen to the northeastern South China Sea; in the northeastern South China Sea, respectively. (▲ denotes the coastal ocean experimental station; x denotes the fully automatic spectra acquisition; and ● denotes the water samples collection).

the sea surface as [6], [33], [35], [36]:

$$R_{rs}(\lambda) = \frac{L_w(\lambda)}{E_s(\lambda)} = \frac{\rho_p[L_{sw}(\lambda) - \delta L_{sky}(\lambda)]}{\pi L_p(\lambda)} \tag{9}$$

where $L_{sw}(\lambda)$ is the upwelling radiance from water, $L_{sky}(\lambda)$ is the downwelling radiance of skylight, $L_p(\lambda)$ is upwelling the radiance from the reference panel, δ is a proportionality coefficient that relates $L_{sky}(\lambda)$ to the reflected sky radiance determined when the detector viewed the water surface, and ρ_p is the irradiance reflectance of the reference panel.

In order to verify the applicability of the system, classical and typical algorithms for deriving Chl-a concentrations are employed in the study, which have been used in the studies by Mao and Pan [37], Xu *et al.* [38], and O'Reilly *et al.* [39].

Referring to the settings of SeaWIFS OC4v4 [39] and MODIS OC3M [40], the algorithm for deriving Chl-a concentrations in the coastal waters of China is taken into account of the logarithmic polynomial form of band ratio with the following expressions:

$$\lg(Chla) = a_0 + a_1 \lg(x) + a_2 \lg(x^2) + a_3 \lg(x^3) \tag{10}$$

$$x = R_{rs}(490)/R_{rs}(550) \tag{11}$$

$$a_0 = 0.9361, \quad a_1 = 23.6498,$$
$$a_2 = 208.8090, \quad a_3 = 506.8767 \tag{12}$$

Compared with the classic OC2 [39] and OC4 [39] algorithms for Chl-a concentrations, the algorithm for Chl-a concentrations used in Case I waters of the South China Sea is more accurately adaptive [37], [38], which is expressed as [37], [38]:

$$Chla = 1.3905\left[L_{wn}(443)/L_{wn}(555)\right]^{-1.6244} \tag{13}$$

For the comparison purposes, the seawater samples were also collected from the sites and analyzed by spectrophotometry using a Cary 5000 UV-Vis-NIR spectrophotometer (Agilent, Inc., Santa Clara, USA), according to the NASA ocean optics protocols [41].

A. EXPERMENTS IN THE COASTAL WATERS OF QINGDAO

For the experiments carried out at coastal ocean experimental station from September 11, 2018 to March 17, 2019, the sky was either clear with little cloud cover or completely covered by clouds. The sea state was generally calm (i.e. level three or below) with very small waves observed and the lighting conditions were uniform. During the experiments, which were conducted over the autumn and winter seasons, the weather conditions were good with very light precipitation.

1) SPECTRA ACQUISITION

The system undertook the daily collection of spectral data automatically. The accuracy and reliability of spectra collected by the system are verified through the comparisons with the measured from the manual spectra acquisition.

Fig.15 shows the spectra of the reference panel, skylight and seawater collected by the system from 2:00 pm to 14:30 on November 16, 2018, in comparison with those obtained from the synchronous manual spectra acquisition. The results show that the variations of the intensity of spectra

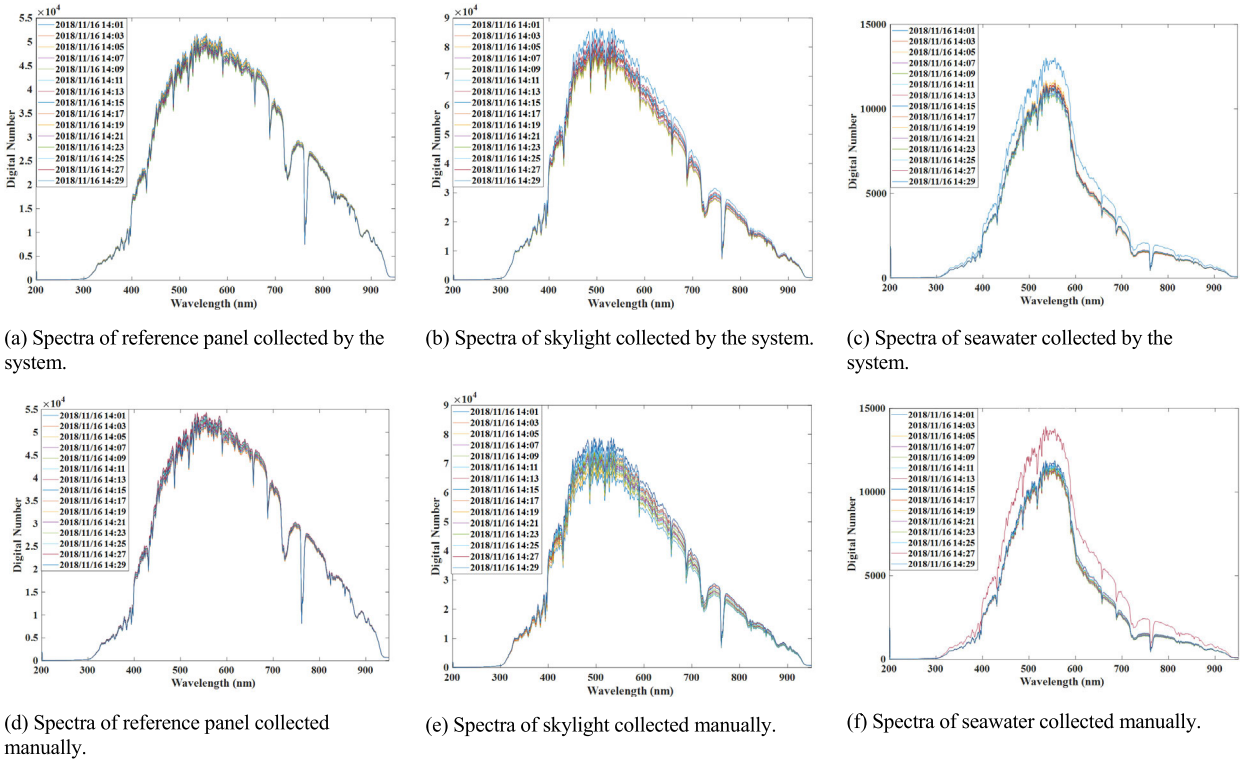

(a) Spectra of reference panel collected by the system.

(b) Spectra of skylight collected by the system.

(c) Spectra of seawater collected by the system.

(d) Spectra of reference panel collected manually.

(e) Spectra of skylight collected manually.

(f) Spectra of seawater collected manually.

FIGURE 15. Comparisons of spectra collected.

collected by the system for the skylight, reference panel and seawater over the range of the wavelength, which agrees well with those measured from the manual acquisition in both magnitude and trend.

Table 5 lists the typical mean values of the spectra in terms of digital numbers (DN) at 4 selected wavelengths averaged over 15 measurements from both the system and manual acquisition, and their relative errors. It is clear that the relative errors of DN values of the reference panel, skylight and seawater are all less than 5% in the four bands, which illustrates satisfactory performance and accuracy of the system in the spectral collection, and demonstrates the reliability and effectiveness of the system as the replacement of manual spectra collection.

TABLE 5. Typical values of the spectra (digital numbers) at selected wavelengths.

Object	Wavelength (nm)	Manual Acquisition	System	Relative Error (%)
Reference panel	400	10137	10421	2.72
	500	41725	41364	0.87
	600	48913	49758	1.69
	700	26342	26179	0.62
Skylight	400	20936	21172	1.11
	500	73548	71907	2.28
	600	66481	64179	3.58
	700	39743	39175	1.45
Seawater	400	1346	1297	3.77
	500	8457	8129	4.03
	600	5978	5812	2.85
	700	2478	2391	3.63

2) REMOTE SENSING REFLECTANCE

In order to further assess the accuracy of the system, the remote sensing reflectance data calculated from spectra collected by the system on December 13, 2018 are compared with that measured by the manual acquisition as shown in Fig.16.

From Fig.16, it is clear that the variations of the remote sensing reflectance obtained from both the system and manual acquisition are highly similar and agree well through the entire range of wavelength. The remote sensing reflectance shows an upward trend in the wavelength range less than almost 500 nm, reaching to a plateau after, and sharply decreases in the wavelength range of 550 nm to 750 nm, which is highly consistent with the trend of Case II waters.

Taking the measured reflectance at 6 particular wavelengths (400 nm, 500 nm, 600 nm, 700 nm, 800 nm and 900 nm respectively) for quantitative comparisons and relative errors analysis, Fig.17 shows the maximum, minimum and average reflectance and relative errors, which show good agreements and the relative errors of the mean values are less than 5%. This result further verified that the system could well achieve the replacement work of manual spectra

TABLE 6. Comparative analysis of Chl-a concentrations obtained by the fully automatic system (System) and measured by the Chl-a monitoring sensor (Sensor).

Time	January 22 12:00	January 23 12:00	January 24 12:00	January 25 12:00	January 26 12:00	January 27 12:00	January 28 12:00
System (mg/m³)	1.2519	1.1392	1.0173	0.9875	1.0517	1.1236	1.2539
Sensor (mg/m³)	1.2937	1.1785	1.0428	1.0131	1.0014	1.2371	1.3921
Relative error (%)	3.23	3.33	2.44	2.52	5.02	9.17	9.93

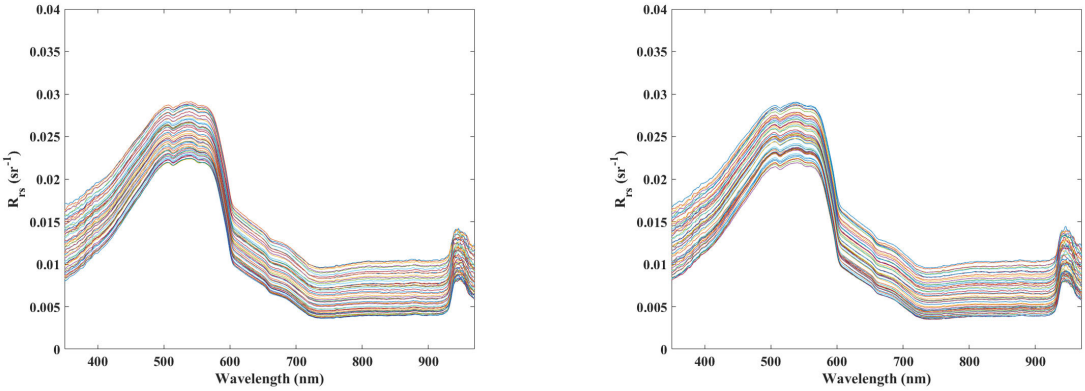

(a) The system (b) The manual acquisition.

FIGURE 16. Remote sensing reflectance calculated from the spectra measured.

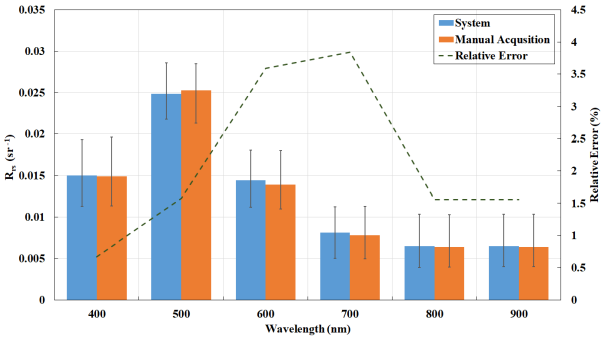

FIGURE 17. The remote sensing reflectance measured by the system and manual acquisition; and the relative errors.

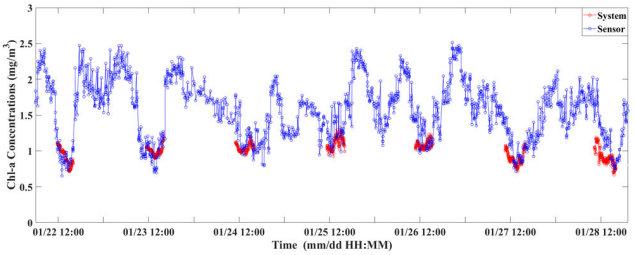

FIGURE 18. Comparisons of Chl-a concentrations obtained by the system (System) and the Chl-a sensor (Sensor).

acquisition, and its accuracy could meet the requirements of spectra measurement.

3) CHL-A CONCENTRATIONS

The reliability and accuracy of the system in determining the Chl-a concentration are the key factors in the system development. The verification is carried out by comparing the Chl-a concentration derived from the spectra collected by the system with that measured by a Chl-a monitoring sensor over a 188-day period of experiments (from January 22, 2019 to January 28, 2019). Fig.18 shows that the trend of the Chl-a concentration calculated from the spectra collected by the system in comparison with those measured by the Chl-a monitoring sensor. It should be noted that the system was only operated with the day time from 09:00 to 16:00. The system shows the same trend as the Chl-a monitoring sensor during the same observation time, and in general a good agreement is achieved.

In order to quantitatively analyze the accuracy of the Chl-a concentration obtained by the system, the data measured at noon of each day during the observation period are selected for error analysis. The results are shown in Table 6. It can be seen from Table 6 that the Chl-a concentration estimated by the system agrees well with that measured by the Chl-a sensor, with the relative errors being less than 10%, and the relative errors of Chl-a concentrations between January 22 and 25 are all less than 5%. This clearly indicates the high accuracy achieved in measuring the Chl-a concentration by the system.

To further demonstrate the accuracy and reliability of the system, in-situ water samples were collected in the coastal

waters where the system performed spectra collection from March 13, 2019 to March 17, 2019 for the inter-comparison purposes. In addition, the manual spectra collection and the measurements from Chl-a sensor were carried out simultaneously, which provide strong comparisons. For the in-situ water samples collected, the spectrophotometric method [41] was used to obtain the Chl-a concentrations in this area, which is regarded as the reference concentration of Chl-a in comparison with those obtained from the spectra collected by both the system and manual acquisition. Fig.19 shows the comparison of the Chl-a concentrations obtained from all 4 methods as described.

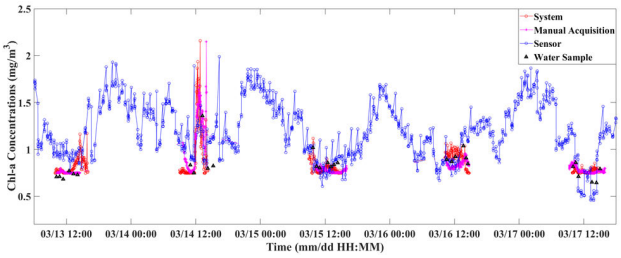

FIGURE 19. Comparative analysis of Chl-a concentrations obtained from the system, manual acquisition, Chl-a monitoring sensor and water sample.

As shown in Fig.19, the trend of the Chl-a concentration obtained by the system is consistent with the trend of Chl-a concentrations retrieved by the manually collected spectra and the trend of the Chl-a concentration measured by the Chl-a sensor. The Chl-a concentration of the three showed an upward or downward trend at the same time. Except for some special cases, the Chl-a concentration of water samples measured in the laboratory was consistent with that of the system, and the deviations were relatively small. In order to further quantitatively analyze the deviation of the Chl-a concentration obtained by the system and the Chl-a concentration obtained from the measured water samples, the error analysis was carried out. The results are shown in Fig.20. It can be seen from Fig.20 that the relative errors between the Chl-a concentration retrieved by the system and that measured from the water samples were less than 10% in most cases. The number of samples with a relative error of less than 10% accounts for 87.1% of the total samples. The number of samples with a relative error of less than 5% accounts for 58.1% of the total samples. The results also validated the reliability, validity, and accuracy of the spectra collected by this system, which means the spectral data collected by the system automatically was able to reflect the actual spectral data.

B. EXPERMENTS ONBOARD THE DONGFANGHONG 3

After the 188-day experiments at the coastal ocean experimental station in Qingdao, the system was onboard the Dongfanghong 3 for further experimental verification of the system performance. During the period of navigation and docking experiments on Dongfanghong 3 scientific research

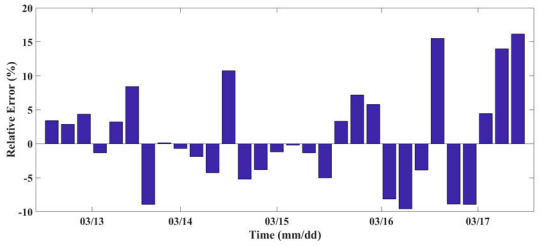

FIGURE 20. Relative errors of Chl-a concentrations between spectra retrieval and water sample measurement.

vessel, the system had conducted continuous spectra acquisition from 9:00 to 16:00. Once the scientific research vessel was suspended, the experiments of water sample collection and filtration treatment were carried out. At the same time, the time, geographic location, weather and other information were recorded simultaneously. While the scientific research vessel was docked, the Chl-a sensor measurements were continued.

1) REMOTE SENSING REFLECTANCE IN DIFFERENT SEA AREAS

Fig.21 shows the remote sensing reflectance of the waters over the wavelength along the Dongfanghong 3 routes.

During the course of the scientific research vessel from coastal to offshore waters, as shown in the Fig.21 (a) and (e), the remote sensing reflectance contain both curves that meet the characteristics of the Case II waters and curves that meet the characteristics of the Case I waters [38]. This is in line with the actual situation, which indicates this should be the water quality transition region. The remote sensing reflectance in the East China Sea area shows a downward trend after a small increase, as shown in Fig.21 (b). The remote sensing reflectance of the South China Sea shows a downward trend as the wavelength increases, as shown in Fig.21 (c) and (f), which is in line with the general trend of the remote sensing reflectance of the Case I waters [42]. In Fig.21 (d), the remote sensing reflectance shows a trend of rising first and then decreasing in coastal waters of Xiamen. It is in line with the overall trend of the remote sensing reflectance in Case II waters [38]. According to the above analysis, it was evidenced that the system onboard the vessel was capable of carrying out long-term spectra collection at different sea areas, and the collected spectral data accurately reflected the actual spectra situation and was regarded as reliable and effective.

2) CHL-A CONCENTRATIONS FROM CASE II WATERS TO CASE I WATERS

To further determine the accuracy of the spectral data collected by the system, the Chl-a concentration retrieval calculation was performed on the spectral data collected by the system. The changing of Chl-a concentrations during the course of scientific research vessel from coastal to offshore waters was analyzed.

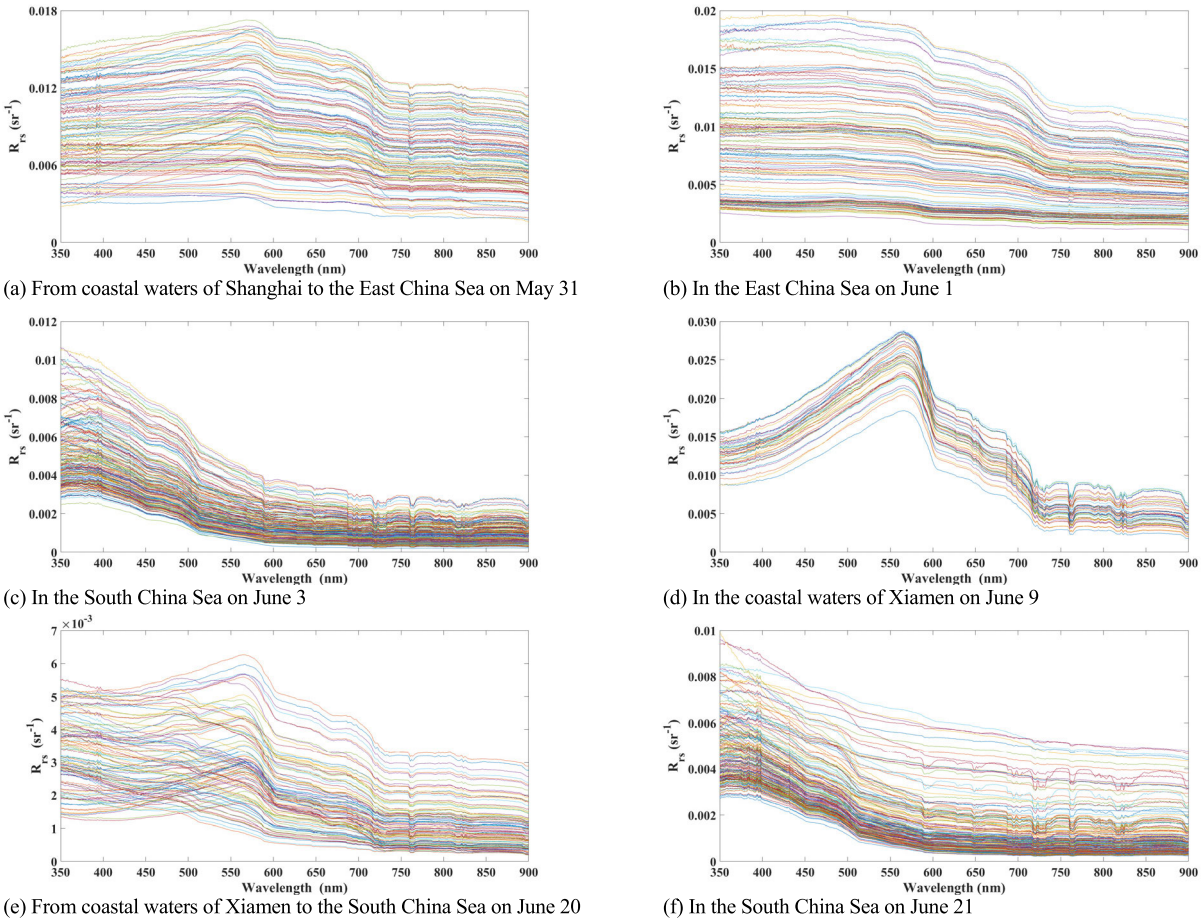

(a) From coastal waters of Shanghai to the East China Sea on May 31
(b) In the East China Sea on June 1
(c) In the South China Sea on June 3
(d) In the coastal waters of Xiamen on June 9
(e) From coastal waters of Xiamen to the South China Sea on June 20
(f) In the South China Sea on June 21

FIGURE 21. Remote sensing reflectance of the waters along the route of the Dongfanghong 3 voyage in 2019.

TABLE 7. Chl-a concentrations obtained from Xiamen coastal water treatment.

Sampling Time	Volume of Filtered seawater (L)	Volume of extract liquid (mL)	Value of optical density				Chl-a concentrations (mg/m^3)
			OD 750	OD 664	OD 647	OD 630	
June 20 9:30	3.00	10.00	0.002	0.075	0.027	0.023	2.7496
June 20 10:20	3.00	10.00	0.002	0.051	0.018	0.014	1.8502

According to the analysis of actual experience, it can be preliminarily determined that the Chl-a concentration in coastal waters should be significantly higher than that in offshore waters. The routes of the scientific research vessel sailing from the Case II waters to Case I waters include the route from the coastal waters of Shanghai to the East China Sea on May 31, the route from the coastal waters of Xiamen to the South China Sea on June 2 and June 20. Therefore, the 3-day spectral observation data was selected for retrieval analysis of Chl-a concentrations. The result was used to analyze whether the Chl-a concentration obtained by spectral retrieval showed a downward trend along with the scientific research vessel's navigation.

It can be seen from Fig.22 that Chl-a concentrations obtained from the retrieval of spectra collected by the system generally show a downward trend from coastal waters to offshore waters, which agrees with the field observation. Moreover, the Chl-a concentration in the East China Sea obtained from the retrieval is about 1.4 mg/m^3 (Fig.22 (a)), and the Chl-a concentration in the South China Sea is about 0.5 mg/m^3 (Fig.22 (b) and (c)), which agree with those observed in literatures [42]–[44]. In addition, surface water samples (0-50 cm) were collected while the spectra were being collected. However, limited by the field test environment, it was not possible to collect water samples while the scientific research vessel was sailing. In the routes shown in Fig.22, two sets of water samples were collected on June 20. The results of Chl-a concentrations from the water samples are shown in Table 7. As can be seen from Table 7, the measured Chl-a concentrations of water samples are basi-

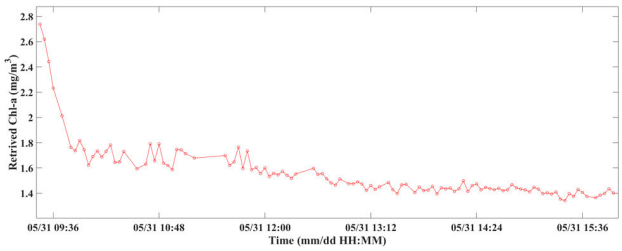

(a) From coastal waters of Shanghai to the East China Sea on May 31

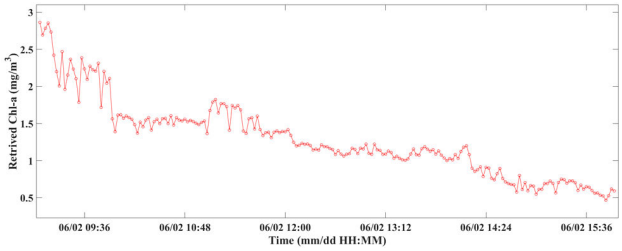

(b) From coastal waters of Xiamen to the South China Sea on June 2

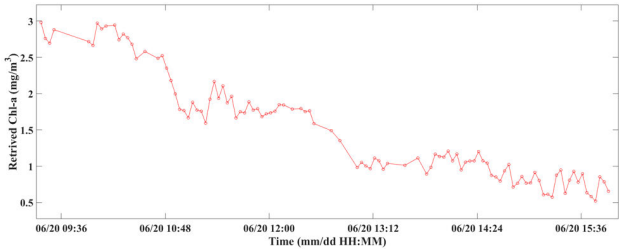

(c) From coastal waters of Xiamen to the South China Sea on June 20

FIGURE 22. **Chl-a concentrations derived from the spectra collected.**

cally consistent with that obtained by retrieval of the spectral measurement. This further demonstrates the reliability, effectiveness, and accuracy of the system's spectral acquisition.

3) CHL-A CONCENTRATIONS IN THE SOUTH CHINA SEA

During the experiment of the scientific research vessel in the South China Sea, spectra collection was continuously carried out by the system from 9:00 to 16:00 every day. When the scientific research vessel was docked for experimental work, the measurement of Chl-a sensors and the collection of water samples were simultaneously performed in situ. The Chl-a concentration retrieved by the system, the Chl-a concentration measured by the Chl-a sensor and the Chl-a concentration obtained from processing the water sample were obtained and compared in Fig.23.

It can be seen from Fig.23 that the Chl-a concentration derived from the system and measured by the sensor show the same patterns of variation. In the long-term observation experiment, the trend of the Chl-a concentration obtained from retrieval of the spectra collected by the system is highly consistent with that measured by the Chl-a sensor during the selected time period. All the Chl-a concentration retrieved by the system are in the range of 0∼0.15 mg/m^3,

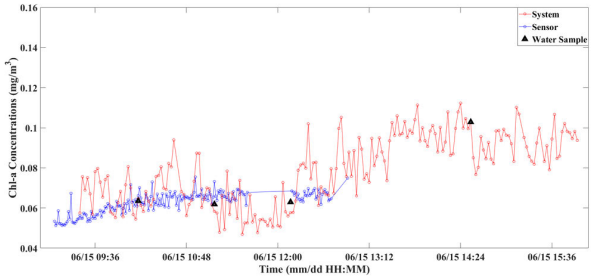

(a) On June 15.

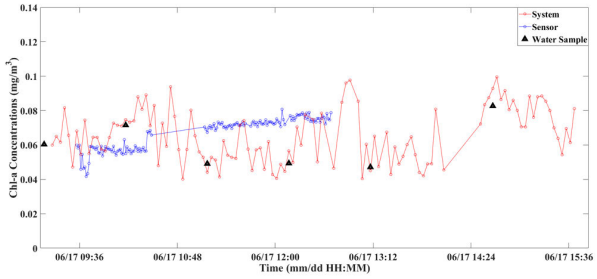

(b) On June 17.

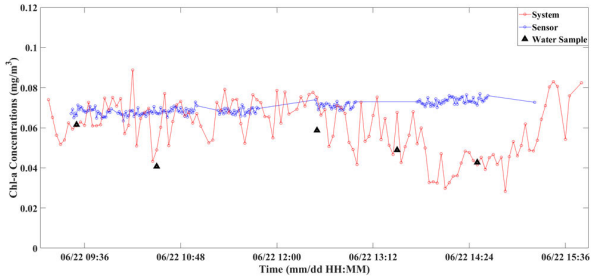

(c) On June 22.

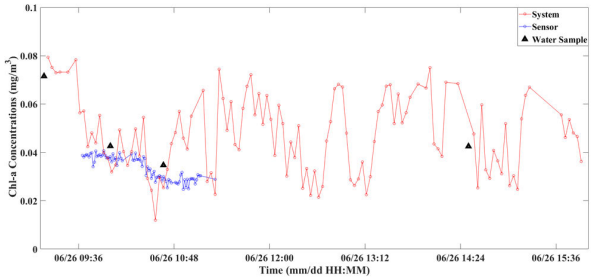

(d) On June 26.

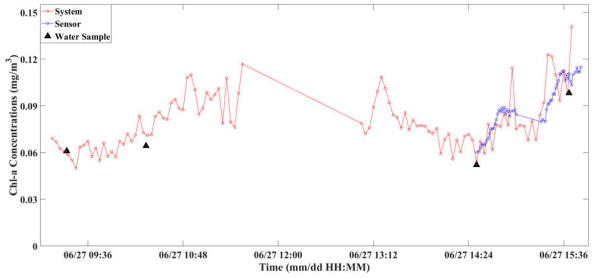

(e) On June 27.

FIGURE 23. **Comparison of Chl-a concentrations in the South China Sea in 2019.**

which agreed with the results from the literature in the South China Sea [45]–[48]. In addition, the Chl-a concentration obtained from the retrieval of the spectra collected by the system are basically consistent with the measured Chl-a concentration of the water samples.

The results of comparative analysis for relative errors are shown in Fig.24. The relative error of the Chl-a concentration retrieved by the system and the measured Chl-a concentration of the water samples is less than 25%. The number of samples with an error less than 20% accounts for 95.65% of the total number of samples. The number of samples with an error less than 10% accounts for 82.6% of the total number of samples. It is clearly demonstrated from the analysis that the Chl-a concentration retrieved by the system has high accuracy and low relative errors, which can truly reflect the actual Chl-a concentration of the observed sea area, hence the accuracy, reliability and effectiveness of the system are further verified.

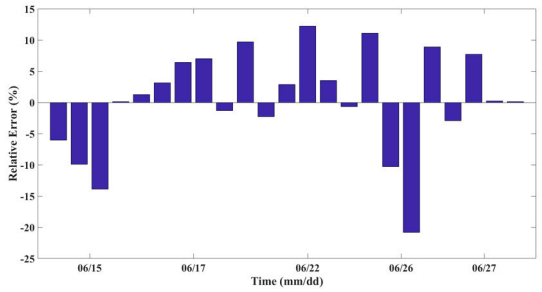

FIGURE 24. Relative errors of Chl-a concentrations between spectra retrieval and water sample measurements in the South China Sea.

VI. CONCLUSION

In this article, a novel fully automatic ocean spectra acquisition and control system based on the real-time solar angle analyzing and tracking is proposed and described.

The newly-designed system is capable of accurately calculating the solar angle by using the information of latitude, longitude, date, and time collected and realizing the automation of adjusting the position of the observation plane of the instrument and the pointing angle of the fiber optic probe in real-time. The rotation of the fiber optic probe is controlled to collect the downstream radiance of skylight, upstream radiance from reference panel and seawater separately, to enable the full automation in acquisition of the ocean spectra. The realization of automatic unattended function makes it possible for the system to carry on a long time continuous spectral observation in a wide range on the marine comprehensive scientific research vessels.

Experimental tests were conducted to verify the performance of the fully automatic ocean spectra acquisition and control system at the coastal ocean experimental station, as well as onboard the comprehensive marine scientific research vessel. The results demonstrated the efficient and stable workflow, the high reliability and accuracy of the system, excellent consistency and stability in both long-term continuous fixed-point measurements, and the applicability across different waters.

The realization of the system would probably bring the following important contributions for the global spectra researchers: (1) The fully automation of the system greatly liberate the manpower in the spectra collection process. Compared with traditional manual spectra collection, it only requires fewer researchers to participate or does not require the participation of researchers. (2) The system can achieve long-term continuous work, which could bring researchers a large amount of data. A large amount of data can cover a wider research area. This solves the problem of insufficient data and small coverage of research area during the manual spectra collection. In general, this system allows researchers to obtain a large amount of data in a wider research area with little manpower.

Although the system has achieved full automation of spectra acquisition, there are still some areas that need to be improved in the system. During the spectra collection, the protection of the reference panel is very important, but we have not achieved a very effective protection method in the design. When the temperature difference between day and night is large in the collection environment, water droplets are prone to condensation on the optical protection objective lens, which affects the accuracy of spectrum collection. These are all areas that need further improvement. The collection of spectra is the first step of remote sensing. In this article, we mainly focus on the design of automatic spectra collection. We have not conducted in-depth research on the inversion algorithm of spectra. Different sea areas need to adopt different algorithms, which is this article needs to do. In addition, The system can also be further improved in the areas of the modular design, low power consumption, miniaturization, easy maintenance and optimization.

In the future, we will further develop these areas that need to be improved for the system. We will initially consider using a dynamic sealing protection box to protect the reference panel, and using resistance wire heating to solve the problem of condensation on the objective lens. We will further study the spectra inversion algorithm for the system to obtain more accurate and effective concentrations of Chl-a in different sea areas. We believe that the automatic large-scale continuous collection of spectra realized by this system will provide researchers with a large amount of effective remote sensing data, and will promote the research and development of ocean color remote sensing.

ACKNOWLEDGMENT

The authors express gratitude to the experimental platform provided by the coastal ocean experimental station and the Dongfanghong 3 comprehensive marine scientific research vessel. Thanks to all those who provided help for the system field experiments. The authors would like to appreciate all the editors and reviewers for their insights and suggestions.

REFERENCES

[1] A. Morel and L. Prieur, "Analysis of variations in ocean color1," *Limnol. Oceanogr.*, vol. 22, no. 4, pp. 709–722, Jul. 1977.

[2] R. K. Singh and P. Shanmugam, "A multidisciplinary remote sensing ocean color sensor: Analysis of user needs and recommendations for future developments," *IEEE J. Sel. Topics Appl. Earth Observ. Remote Sens.*, vol. 9, no. 11, pp. 5223–5238, Nov. 2016.

[3] D. D'Alimonte, T. Kajiyama, and A. Saptawijaya, "Ocean color remote sensing of atypical marine optical cases," *IEEE Trans. Geosci. Remote Sens.*, vol. 54, no. 11, pp. 6574–6586, Nov. 2016.

[4] P. V. Nagamani, P. Chauhan, and R. M. Dwivedi, "Development of chlorophyll-*a* algorithm for ocean colour monitor onboard OCEANSAT-2 satellite," *IEEE Geosci. Remote Sens. Lett.*, vol. 5, no. 3, pp. 527–531, Jul. 2008.

[5] K. Bai, N.-B. Chang, and C.-F. Chen, "Spectral information adaptation and synthesis scheme for merging cross-mission ocean color reflectance observations from MODIS and VIIRS," *IEEE Trans. Geosci. Remote Sens.*, vol. 54, no. 1, pp. 311–329, Jan. 2016.

[6] D. Jiang, B. Matsushita, and W. Yang, "A simple and effective method for removing residual reflected skylight in above-water remote sensing reflectance measurements," *ISPRS J. Photogramm. Remote Sens.*, vol. 165, pp. 16–27, Jul. 2020.

[7] Z. Ping Lee, W. J. Rhea, R. Arnone, and W. Goode, "Absorption coefficients of marine waters: Expanding multiband information to hyperspectral data," *IEEE Trans. Geosci. Remote Sens.*, vol. 43, no. 1, pp. 118–124, Jan. 2005.

[8] P. Cipollini, G. Corsini, M. Diani, and R. Grasso, "Retrieval of sea water optically active parameters from hyperspectral data by means of generalized radial basis function neural networks," *IEEE Trans. Geosci. Remote Sens.*, vol. 39, no. 7, pp. 1508–1524, Jul. 2001.

[9] H. Chen, F. Yin, W. Huang, M. Liu, and D. Li, "Ocean surface drifting buoy system based on UAV-enabled wireless powered relay network," *Sensors*, vol. 20, no. 9, p. 2598, May 2020.

[10] B. Liu, Z. Fan, and X. Wang, "Solar position acquisition method for polarized light navigation based on ∞ characteristic model of polarized skylight pattern," *IEEE Access*, vol. 8, pp. 56720–56729, 2020.

[11] F. S. Marzano, V. Mattioli, L. Milani, K. M. Magde, and G. A. Brost, "Sun-tracking microwave radiometry: All-weather estimation of atmospheric path attenuation at *Ka* -, *V* -, and *W* -Band," *IEEE Trans. Antennas Propag.*, vol. 64, no. 11, pp. 4815–4827, Nov. 2016.

[12] Z. Zhen, Z. Zengwei, S. Li, W. Jun, P. Wuchun, L. Zhikang, W. Lei, C. Wei, and S. Yunhua, "The effects of inclined angle modification and diffuse radiation on the sun-tracking photovoltaic system," *IEEE J. Photovolt.*, vol. 7, no. 5, pp. 1410–1415, Sep. 2017.

[13] D. A. Flores-Hernandez, S. I. Palomino-Resendiz, A. Luviano-Juarez, N. Lozada-Castillo, and O. Gutierrez-Frias, "A heuristic approach for tracking error and energy consumption minimization in solar tracking systems," *IEEE Access*, vol. 7, pp. 52755–52768, 2019.

[14] W. W. Li, Y. N. Zhang, X. B. Zheng, X. Li, and E. C. Liu, "Design and test of automatic sun-tracking device for solar irradiance spectroradiometer," *J. Atmos. Environ. Opt.*, vol. 8, no. 3, pp. 232–240, 2013.

[15] X. N. Chen, L. Zhang, J. G. Liu, T. S. Zhang, G. Z. Yu, and F. Wu, "Research and implement of the automatic spectrum collecting system based on the sun tracking," *Acta Energiae Solaris Sinica*, vol. 34, no. 5, pp. 800–804, 2013.

[16] D. R. Mishra, B. A. Schaeffer, and D. Keith, "Performance evaluation of normalized difference chlorophyll index in northern gulf of mexico estuaries using the hyperspectral imager for the coastal ocean," *GISci. Remote Sens.*, vol. 51, no. 2, pp. 175–198, Mar. 2014.

[17] G. Tilstone, G. Dall'Olmo, M. Hieronymi, K. Ruddick, M. Beck, M. Ligi, M. Costa, D. D'Alimonte, V. Vellucci, D. Vansteenwegen, A. Bracher, S. Wiegmann, J. Kuusk, V. Vabson, I. Ansko, R. Vendt, C. Donlon, and T. Casal, "Field intercomparison of radiometer measurements for ocean colour validation," *Remote Sens.*, vol. 12, no. 10, p. 1587, May 2020, doi: 10.3390/rs12101587.

[18] N. W. Dahl, P. L. Woodfield, C. J. Lemckert, H. Stratton, and A. Roiko, "A practical model for sunlight disinfection of a subtropical maturation pond," *Water Res.*, vol. 108, pp. 151–159, Jan. 2017.

[19] A. Simon and P. Shanmugam, "A model to predict spatial, spectral and vertical changes in the average cosine of the underwater light fields: Implications for remote sensing of shelf-sea waters," *Continental Shelf Res.*, vol. 116, pp. 27–41, Mar. 2016.

[20] O. D. Maliani, A. Bekkaoui, E. H. Baali, K. Guissi, Y. El Fellah, and R. Errais, "Investigation on novel design of solar still coupled with two axis solar tracking system," *Appl. Thermal Eng.*, vol. 172, May 2020, Art. no. 115144, doi: 10.1016/j.applthermaleng.2020.115144.

[21] K. K. Chong and C. W. Wong, "General formula for on-axis sun-tracking system and its application in improving tracking accuracy of solar collector," *Sol. Energy*, vol. 83, no. 3, pp. 298–305, Mar. 2009.

[22] C. X. Du, P. Wang, C. F. Ma, and Y. T. Wu, "The application of day number in calculating the solar position," *Acta Energiae Solaris Sinica*, vol. 32, no. 11, pp. 1640–1645 2011.

[23] H. N. Ding and X. Li, "Research of dish-type solar thermal power generation tracking control system," *J. Electron. Meas. Instrum.*, vol. 33, no. 4, pp. 202–209, 2019.

[24] M.-C. Ho, A.-C. Lai, K.-K. Chong, M.-H. Tan, B.-H. Lim, Y.-J. King, and J.-V. Lee, "Design and construction of prototype mobile sun-tracking system for concentrator photovoltaic system," *Energy Procedia*, vol. 142, pp. 736–742, Dec. 2017.

[25] A. Rawat, S. K. Jha, and B. Kumar, "Position controlling of sun tracking system using optimization technique," *Energy Rep.*, vol. 6, pp. 304–309, Feb. 2020.

[26] A. Awasthi, A. K. Shukla, M. M. S. R., C. Dondariya, K. N. Shukla, D. Porwal, and G. Richhariya, "Review on sun tracking technology in solar PV system," *Energy Rep.*, vol. 6, pp. 392–405, Nov. 2020.

[27] Y. Zhu, J. Liu, and X. Yang, "Design and performance analysis of a solar tracking system with a novel single-axis tracking structure to maximize energy collection," *Appl. Energy*, vol. 264, Apr. 2020, Art. no. 114647, doi: 10.1016/j.apenergy.2020.114647.

[28] G. A. Wang, H. T. Mi, T. H. Deng, Y. N. Li, and L. X. Li, "Calculation of the change range of the sun high angle and the azimuth of sunrise and sunset in one year," *Meteorolog. Environ. Sci.*, vol. 30, no. S1, pp. 161–164 2007.

[29] K. L. Carder and R. G. Steward, "A remote-sensing reflectance model for red-tide dinoflagellate off West Florida," *Limnol. Oceanogr.*, vol. 30, no. 2, pp. 286–298, 1985.

[30] A. Lababpour and C.-G. Lee, "Simultaneous measurement of chlorophyll and astaxanthin in haematococcus pluvialis cells by first-order derivative ultraviolet-visible spectrophotometry," *J. Biosci. Bioeng.*, vol. 101, no. 2, pp. 104–110, Feb. 2006.

[31] R. J. W. Brewin, G. Dall'Olmo, S. Pardo, V. van Dongen-Vogels, and E. S. Boss, "Underway spectrophotometry along the atlantic meridional transect reveals high performance in satellite chlorophyll retrievals," *Remote Sens. Environ.*, vol. 183, pp. 82–97, Sep. 2016.

[32] C. J. Lorenzen, "Determination of chlorophyll and pheo-pigments: Spectrophotometric equations1," *Limnol. Oceanogr.*, vol. 12, no. 2, pp. 343–346, Apr. 1967.

[33] C. D. Mobley, "Estimation of the remote-sensing reflectance from above-surface measurements," *Appl. Opt.*, vol. 38, no. 36, pp. 7442–7455, Dec. 1999.

[34] K. Uudeberg, A. Aavaste, K.-L. Köks, A. Ansper, M. Uusõue, K. Kangro, I. Ansko, M. Ligi, K. Toming, and A. Reinart, "Optical water type guided approach to estimate optical water quality parameters," *Remote Sens.*, vol. 12, no. 6, p. 931, Mar. 2020.

[35] J. Xu, C. Gao, and Y. Wang, "Extraction of spatial and temporal patterns of concentrations of chlorophyll—A and total suspended matter in poyang lake using GF-1 satellite data," *Remote Sens.*, vol. 12, no. 4, p. 622, Feb. 2020.

[36] J. L. Mueller and R. W. Austin, "Ocean optics protocols for SeaWiFS validation," in *SeaWiFS Technical Report Series*, vol. 5. Washington, DC, USA: NASA, 1992.

[37] Z. H. Mao and D. L. Pan, "Inversion model of satellite-measured chlorophyll a concentration for case 1 waters in China sea," *High Technol. Lett.*, pp. 86–89, 2003.

[38] D. Z. Xu, W. X. Cao, and G. F. Wang, "A bio-optical model for retrieval of chlorophyll-a concentration in northern South China Sea," *J. Tropical Oceanogr.*, vol. 26, no. 2, pp. 15–21, 2007.

[39] J. E. O'Reilly, S. Maritorena, and D. A. Siegel, "Ocean color chlorophyll a algorithms for SeaWiFS, OC2, and OC4: Version 4," in *SeaWiFS Post-launch Calibration and Validation Analyses, Part 3*, S. B. Hooker and E. R. Firestone, Eds. Greenbelt, MD, USA: NASA Goddard Space Flight Center, 2000, pp. 9–23.

[40] K. Chakraborty, A. Gupta, A. A. Lotliker, and G. Tilstone, "Evaluation of model simulated and MODIS-Aqua retrieved sea surface chlorophyll in the eastern arabian sea," *Estuarine, Coastal Shelf Sci.*, vol. 181, pp. 61–69, Nov. 2016.

[41] J. L. Mueller, G. S. Fargion, and C. R. McClain, "Inherent optical properties: Instruments, characterizations, field measurements and data analysis protocols," in *Ocean Optics Protocols For Satellite Ocean Color Sensor Validation, Revision*, vol. 4. Washington, DC, USA: NASA, 2003.

[42] S. Wang, S. Li, J. Hu, and B. Geng, "Experiments in optimizing simulations of the subsurface chlorophyll maximum in the South China sea," *J. Mar. Syst.*, vol. 156, pp. 1–15, Apr. 2016.
[43] Y. Yu, X. Xing, H. Liu, Y. Yuan, Y. Wang, and F. Chai, "The variability of chlorophyll—A and its relationship with dynamic factors in the basin of the south China sea," *J. Mar. Syst.*, vol. 200, Dec. 2019, Art. no. 103230, doi: 10.1016/j.jmarsys.2019.103230.
[44] W. Zhang, X. Sun, S. Zheng, M. Zhu, J. Liang, J. Du, and C. Yang, "Plankton abundance, biovolume, and normalized biovolume size spectra in the northern slope of the South China sea in autumn 2014 and summer 2015," *Deep Sea Res. II, Topical Stud. Oceanogr.*, vol. 167, pp. 79–92, Sep. 2019.
[45] C. Zhang, C. Hu, S. Shang, F. E. Müller-Karger, Y. Li, M. Dai, B. Huang, X. Ning, and H. Hong, "Bridging between SeaWiFS and MODIS for continuity of chlorophyll—A concentration assessments off southeastern China," *Remote Sens. Environ.*, vol. 102, nos. 3–4, pp. 250–263, Jun. 2006.
[46] Z. Lu, J. Gan, M. Dai, and A. Y. Y. Cheung, "The influence of coastal upwelling and a river plume on the subsurface chlorophyll maximum over the shelf of the northeastern south China sea," *J. Mar. Syst.*, vol. 82, nos. 1–2, pp. 35–46, Jul. 2010.
[47] Y. Zhang, H. Jiang, C. Chen, X. Y. Zhang, and Y. Wang, "Wavelet analysis on chlorophyll concentration change in the area around bohai bay area, yangtze river delta region and South China sea," *Procedia Environ. Sci.*, vol. 13, pp. 1373–1382, Jan. 2012.
[48] M. Liu, X. Liu, A. Ma, T. Li, and Z. Du, "Spatio-temporal stability and abnormality of chlorophyll—A in the northern south China sea during 2002–2012 from MODIS images using wavelet analysis," *Continental Shelf Res.*, vol. 75, pp. 15–27, Mar. 2014.

LEI YANG received the B.S. and M.S. degrees in communication engineering from the Harbin Institute of Technology, Harbin, China, in 2011 and 2013, respectively. He is currently a Research Scientist with the Institute of Oceanographic Instrumentation, Qilu University of Technology (Shandong Academy of Sciences), Qingdao, China. His research interests include data analysis and processing, system design, remote sensing, and array signal processing.

HAO GAO received the M.S. degree from Newcastle University, Newcastle, U.K., in 2013. He is currently pursuing the Ph.D. degree with the First Institute of Oceanography, Ministry of Natural Resources, Qingdao, China. His research interests include marine environmental monitoring, big data analysis, remote sensing, digital image processing, and deep learning techniques.

DINGFENG YU (Member, IEEE) received the Ph.D. degree in environmental science from the Yantai Institute of Coastal Zone Research, Chinese Academy of Sciences, Yantai, China, in 2013. He is currently an Associate Professor with the Institute of Oceanographic Instrumentation, Qilu University of Technology (Shandong Academy of Sciences), Qingdao, China. He has published some articles on the IEEE journal and IEEE conferences. His main research interests include ocean color remote sensing and signal processing.

SHUNQI PAN received the Ph.D. degree in fluid mechanics from Heriot-Watt University, Edinburgh, U.K., in 1993. He is currently a Professor in coastal engineering and the Director of the Hydro-Environmental Research Centre, School of Engineering, Cardiff University, U.K. He has many years research experience in coastal engineering, including physical and numerical modeling of coastal and estuarine processes. His current research interest includes marine environmental monitoring.

YAN ZHOU received the M.S. degree in marine information detection and processing from the Ocean University of China, Qingdao, China, in 2011. She is currently a Research Assistant with the Institute of Oceanographic Instrumentation, Qilu University of Technology (Shandong Academy of Sciences), Qingdao. Her research interests include remote sensing retrieval and application of ocean color, calibration verification of microwave scatterometers, and comprehensive analysis and processing of ocean remote sensing data.

YINGYING GAI received the B.E. degree in geomatics engineering from the Shandong University of Science and Technology, Qingdao, China, in 2009, and the M.S. degree in photogrammetry and remote sensing from Peking University, Beijing, China, in 2012. She is currently working as an Engineer with the Institute of Oceanographic Instrumentation, Qilu University of Technology (Shandong Academy of Sciences), Qingdao. Her main research interests include ocean color remote sensing, remote sensing image processing, and computer vision.